KERNFORSCHUNGSANLAGE JÜLICH
GESELLSCHAFT MIT BESCHRÄNKTER HAFTUNG
Institut für Festkörperforschung

The Niobium Hydrogen System: An Electron Microscope Study

Part I: Room Temperature Results
Part II: Low Temperature Structures

by

T. Schober

Jül - 1160
Januar 1975

Als Manuskript gedruckt

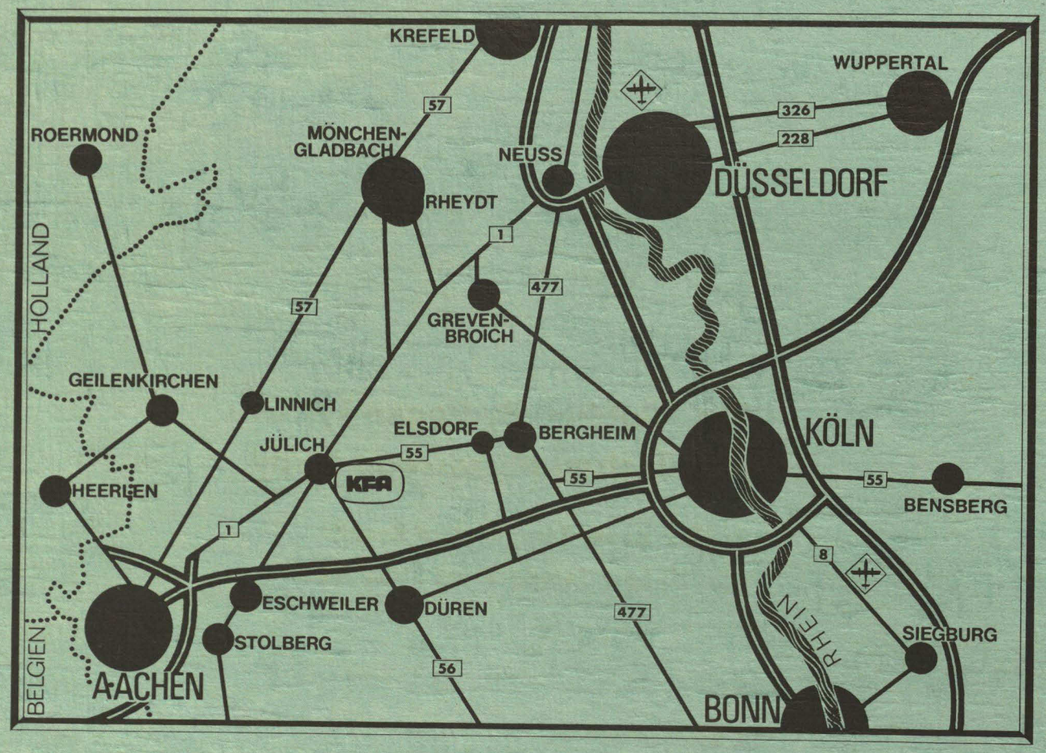

Berichte der Kernforschungsanlage Jülich - Nr. 1160

Institut für Festkörperforschung Jül - 1160

Dok.: Metal-Gas System - Nb-H, Electron Microscopy, Morphologies
Nb-H System - Morphologies, Crystal Defect, Hydride Precipitation
Hydrogen Embrittlement - Niobium
Low Temperature Nb-H Phases
Pricipitation Damage - Niobium

Im Tausch zu beziehen durch: ZENTRALBIBLIOTHEK der Kernforschungsanlage Jülich GmbH,
Jülich, Bundesrepublik Deutschland

The Niobium Hydrogen System: An Electron Microscope Study

Part I: Room Temperature Results

Part II: Low Temperature Structures

by

T. Schober

The Niobium Hydrogen System: An Electron Microscope Study
Part I: Room Temperature Results

T. Schober
Institut für Festkörperforschung,
Kernforschungsanlage Jülich, 517 Jülich

Abstract (Part I)

The room temperature morphology of β- and δ-phase precipitation in the NbH system was investigated under ultrahigh purity conditions (UHV degassed Nb and electrolytic charging). The β-phase ($NbH_{0.7}$ in the two phase region) precipitated after electrolytic charging at room temperature in the form of large, dendritic particles. Charging at 150°C mainly resulted in plates on {100}. The presence of domain boundaries, antiphase boundaries and twins in such precipitates was demonstrated. Evidence for extensive plastic deformation in β-phase areas was obtained and possible reasons for this are discussed. δ-phase (f.c.c. NbH_2) precipitation occurred in the form of plates on {210} inside the β-phase. Observations are presented on the β- and δ-phase morphology for concentrations of up to 200 % (= H/Nb). The main reasons for hydrogen embrittlement in highly charged NbH samples are described.

1. Introduction

The interaction of niobium with interstitially dissolved gases has been a topic of continued interest during recent years. A considerable part of the attention has been focussed on the niobium hydrogen system with its implications for reactor and fusion technology as well as for superconducting cavities. In Part I of this work, transmission and scanning electron microscope (TEM and SEM) results on hydride precipitation in Nb as observable at room temperature are presented. Part II /1/ mainly deals with TEM work on low temperature hydride phases. A brief account of some of the results has appeared elsewhere /2/.

A partial phase diagram of the NbH system is presented in fig. 1 showing the disordered b.c.c. solutions α and α' /3/, the b.c.c. γ-phase /4,5/, the δ-phase of the composition NbH_2 /6/ (in which the Nb atoms are in f.c.c. positions), the ordered orthorhombic β-phase /3 to 5,7,8/ and the ordered solutions ε and ζ which are discussed in Part II of this work /1/. Some TEM observations of β-phase precipitation have been presented before /9 to 11/.

2. Experimental

The experimental details have been fully described elsewhere /2,9/. In brief, UHV-degassed high purity Nb foils of 25 μm thickness were electrolytically hydrogen charged either at room temperature or at approximately 150°C and electropolished /12/[1)].

---

1) In the beginning, a number of TEM samples were produced from NbH alloys as obtained by treatment in a hydrogen atmosphere under ultra pure conditions inside a UHV chamber. It was soon observed that all of these specimens nevertheless showed evidence for the precipitation of contaminants (probably oxygen and nitrogen). For this reason, the use of NbH samples charged from the gas phase was abandoned. Conversely, UHV degassed Nb, which was electrolytically hydrogen charged, guaranteed the complete absence of other gaseous impurities.

The observations were carried out in a Philips EM 300 G electron microscope equipped with a scanning attachment allowing "scanning transmission electron microscopy" (STEM), as well as standard SEM using backscattered electrons. Because of the thermal instability of the hydrides, the TEM work was performed, whenever possible, in the cooling holder at -150°C to -160°C. In this way the room temperature state of hydrogen precipitation (i.e. its morphology) could be frozen in although phase transitions occurred in the internal structure of the hydrides as outlined in Part II /1/. It is emphasized that these low temperature phase transitions did not affect the morphologies present at room temperature.

During the course of this work, it was found that electrolytic charging at both charging temperatures (room temperature and 150°C) led to a rather inhomogeneous distribution of hydrides. For instance, areas of widely differing concentrations of hydrogen were observed in a given specimen. It was possible to charge some portions of a specimen beyond 100 % (H/Nb = 1.0) (where hydrogen embrittlement became a serious problem) while adjacent areas were in the α-β two phase region. Thus,reliable hydrogen concentration values were not available for the observed TEM samples. However, approximate "local concentrations" could be assigned to the various areas from the proportions of the phases present.

For the SEM observations, small Nb single crystal chips (roughly 3 x 3 x 0.5 mm in size) were prepared and also electrolytically hydrogen charged. After loading they were slightly etched (HF and HNO_3 1:1) to enhance the topographic contrast.

3. Results

3.1 α-Phase Observations at Room Temperature

When NbH α-phase regions with c < 5 % were observed by TEM at room temperature, it was noted that extensive elastic buckling and straining occurred in the regions exposed to the focussed electron beam. This effect may be explained by a local gradient

in temperature (induced by the electron beam) which produced a concentration gradient given by (/13/):

$$\frac{\text{grad } c}{c} = -\frac{Q}{kT}\,\frac{\text{grad}T}{T} \qquad (1)$$

where c is the hydrogen concentration, T the temperature, k Boltzmann's constant, and Q the heat of transport (Q = +0.13 eV for Nb /13/). The concentration gradient in turn caused local differences in lattice parameter /5/ and therefore, elastic bending. Thus, regions of the α-phase could easily be recognized through the above bending effects.

3.2 β-Phase Precipitation after Electrolytic Hydrogen Charging

In complete agreement with a recent metallographic study /14/, it was found that room temperature electrolytic charging led to irregularly shaped β-hydride particles with dendritic features. Charging at 150°C produced some dendritic hydrogen precipitates, but mainly plates of the β-hydride phase on {100}. (The latter shape is considered as the "equilibrium" morphology which is always obtained at high charging temperatures, low charging rates and low cooling rates /14/.) In the present study, mostly samples produced by room temperature charging were investigated. The main reason for this was that at room temperature β-phase regions could be produced which had a dislocation density comparable to that of the original Nb foil. Charging at 150°C usually led to β-phase regions which had suffered a considerable amount of plastic deformation (see below).

In fig. 2 the dendritic β-phase morphology after room temperature charging is shown. It is seen that rather large areas of the hydride phase were obtained. Also, the dendritic character of the α-β interface is visible. Here, periodically spaced plates of the β-phase are protruding into the α-phase. When such hydride particles were observed by TEM, their inner parts appeared as large, smooth and homogeneous areas of the β-phase. The periphery, however, looked like a stack of α- and β-phase plates, and often appeared as though periodically spaced plates of the α-phase were embedded in the β-phase /2/.

In a previous paper /9/, a TEM study of Nb β-hydride was presented in which (1) direct evidence for the ordering of hydrogen atoms was obtained, and (2) the ensuing reciprocal lattice (as proposed from neutron diffraction work /15/) was confirmed. Fig. 3a shows the distribution of hydrogen on tetrahedral sites in the orthorhombic β-phase, and fig. 3b the resulting reciprocal lattice. In the β-phase of the two phase region, the hydrogen atoms occupy on the average 3 out of 4 tetrahedral sites leading to a composition of approximately $NbH_{0.7}$ /15/. Due to the incomplete occupancy of the available tetrahedral sites, further ordering can occur at lower temperatures (see Part II /1/).

The most common observations within the β-phase were domain boundaries, as discussed previously /9/. They were usually found to run in a zig-zag fashion through the specimen producing tilts of opposite sign[2]. Trace analysis showed the domain boundaries to have a tendency to lie on low index planes such as {100} - {110} - {111} - {211} and {210}[3),4)] although the boundaries in the thinned samples were much more curved than those observed in bulk -NbH /14/.

Dark field observations using superlattice reflections showed the β-phase to contain antiphase boundaries (APB's) as shown in fig. 4. (For details see figure caption.) Also β-phase hydride, as produced electrolytically at 150°C often was found to contain a large number of very thin twins, with lengths of several microns, and $(211)_{b.c.c.}$ habit planes. Bright and dark field pictures as well as a SAD pattern of such twins are presented in fig. 5a, b, c.

---

2) In this way, no large scale changes in shape of the crystals (with the associated deformations) could arise.

3) Here and in the following, the b.c.c. notation is used. This is permissible because of the very small deviations from the cubic structure which are encountered in the β-phase /5/.

4) It is seen in fig. 3a that these planes correspond to low index planes in the β-phase as well.

3.3 Plastic-Deformation Effects inside β-phase Areas

Inspection of room temperature charged Nb samples revealed the following effects after electropolishing:

1. Optical microscopy and SEM showed that many of the thinner portions of the specimens were badly deformed as witnessed by severe buckling and warping in these areas. The above areas had lost their metallic luster and appeared grey.
2. TEM showed that (aside from smooth low dislocation density areas) there were parts of the β-phase which were permeated by dark bands having a very high dislocation density.
3. At the intersection of such bands, microcracks were commonly observed.
4. On dark field pictures arising from superlattice reflections of the β-phase, the above bands appeared as dark.

The above observations may be explained by the occurrence of extensive plastic deformation in these β-phase areas. On the TEM pictures, the dark bands were generally parallel to the traces of {110}, {112} and {123}, i.e. the traces of slip planes in b.c.c. Nb /16/.

Apparently, slip was confined in such a way as to produce the above bands of deformed material. At the intersections of such slip bands, the plastic strain often was high enough for the formation of microcracks. In fig. 6, a representative TEM picture of the above slip bands inside the β-phase is shown. (Details in Figure Caption). Fig. 7a and b show a bright and dark field picture of a similar deformed area. (Fig. 7b was taken with a β-phase superlattice reflection.) The high dislocation density bands in fig. 7a correspond to the dark stripes in fig. 7b. Apparently, slip has produced slabs in the material where either order has been destroyed, and its restitution prevented by the high dislocation density, or where the dislocation density in the ordered areas is too high to get sufficient intensity for the formation of a dark field image. Probable reasons for the extensive plastic deformation will be given in the Discussion.

3.4 δ-Phase Precipitation

Small single crystal chips could easily be charged at 150°C to the single phase β region (70 % < c < 100 %) at room temperature. If charging was continued, small needles were observed to start growing from the corners of the chips into their centers. The needles were typically a few µm wide and were crystallographically oriented. It is shown below that these needles on the surface represent the growth of δ-phase plates inside the β-phase. The onset of δ-phase precipitation could easily be recognized by a dull and grey appearance of the areas affected (diffuse light scattering at the δ-phase plates). As charging was continued, the δ-phase plates grew throughout the specimen and increased in thickness until thick δ-bands permeated the samples.

In fig. 8a a SEM picture of δ-phase precipitation on a {110} surface is shown; fig. 8b illustrates precipitation on {100}. (Details in Figure Caption). A two surface trace analysis showed the δ-phase plates to lie on {210} planes, which is identical with the habit plane of the δ-phase as determined in a recent metallographic study /14/. In fig. 9, a schematic view of the precipitate morphologies is presented for {100} planes and concentrations from 0 to 200 %.

X-ray powder diffraction on similar samples confirmed the presence of the δ-phase. In agreement with previous studies /6/, the δ-phase was found to have a f.c.c. structure with a = 0.4556 ± 0.0002 nm. δ-phase precipitation caused further plastic deformation of the β-phase areas as witnessed by a large number of cracks in the β-areas. Cracking was found to occur on {110} and, to a lesser extent, on {100} . Unetched samples revealed microcracks also at intersections of δ-phase plates. It was possible to charge some portions of specimens to 170 - to 200 %. Here, thin isolated plates of the β-phase on {210} were remaining, and the areas appeared as if β-phase precipitation had occurred in the "δ-matrix". Attempts to look at δ-phase areas by TEM were unsuccessful. Apparently, the thin specimens became too fragile at such high concentrations and

crumbled prior to observation. Also, a preferential electrolytic dissolution of δ-phase areas was observed.

4. Discussion

The present observations (see also Part II) strongly suggest a diffusion controlled mechanism for the formation of β-phase precipitates and contradict the martensitic transformation model as proposed in /17/. Although the $\alpha \rightarrow \beta$ transformation has some similarities with a bainitic reaction /10/, we agree with the conclusion of Rashid and Scott /18/ that, from the point of view of a metallurgist, β-phase precipitation essentially belongs to a new type of non-classical phase transformation, here referred to as "hydrogen precipitation". The main characteristics of this new metallurgical type of transformation are (1) very high diffusivity of hydrogen in the matrix as well as in the precipitates, (2) the formation of ordered hydrides (which is mainly due to a periodic arrangement of the elastic dipoles associated with the interstitially dissolved hydrogen), and (3) precipitation occurring basically in a "one component" system; the host lattice is only slightly affected by the transformation /19/.

There are a number of possible reasons for the extensive plastic deformation encountered in some portions of the β-phase. Very likely a combination of reasons generally apply to a specific situation and an assessment of the main contributing factor is difficult. As main causes for the β-phase deformation we consider (1) ordering strains arising from the formation of an enlarged orthorhombic structure which lead to a deformation of growing β-phase particles, (2) electrolytic thinning may eliminate some of the elastic constraints which in turn may lead to severe buckling and straining, (3) between 70 and 100 % there is a continuous and monotonic elongation of the orthorhombic unit cell (as expressed by the "shear angle" γ /5/). In the view of the multidomain structure of β-phase crystals /9, 14/, it is easily seen that an increase in the concentration from 70 to 100 % (with the accompanying anisotropic increase in size of the unit cell) will generally lead to plastic

deformation. Thus, provided some portions of the specimen have a concentration higher than 70 %, we would expect them to exhibit plastic deformation effects. (4) A very important factor is the frequently observed inhomogeneities in concentrations which often even lead to cracking of the specimens[5]. (5) Also, there is some evidence that due to the large supersaturations during charging, δ-phase plates are formed which then redissolve. Obviously, precipitation of δ-phase plates, in conjunction with the b.c.c. to f.c.c. transformation, will cause plastic flow in the adjacent β-phase areas. It is also quite probable that some of the high dislocation bands observed in the β-phase were actually "skeletons" of previous δ-phase plates[6].

δ-phase precipitation reflects the inability of the β-phase at roughly 100 % to incorporate further hydrogen. Here for the first time the dissolved hydrogen drastically affects the host lattice and forces it to undergo the b.c.c. to f.c.c. transformation. The {210} habit planes have been observed before in the Nb-O system /21/.

As noted before, highly charged NbH samples were very brittle. As main reasons for this brittleness we consider:

(1) the inherent brittleness of the β-phase itself which may easily be cleaved on {110}.

(2) the formation of microcracks at intersecting slip bands in the β-phase which under the influence of an applied stress may turn into macroscopic cracks.

---

5) These inhomogeneities in concentrations could have easily arisen during room temperature charging where the diffusivity of H in α-Nb is roughly 10^2 x greater than in β-NbH /20/. This could have led to a hydrogen enrichment of the β-phase areas exposed to the electrolyte.

6) It has been demonstrated /6/ that the δ-phase is rather unstable at a vacuum of 10^{-6} Torr and is partially converted into β-NbH. Thus, it is conceivable that substantial "degassing" of hydrogen occurred inside the electron microscope, and that plates of the δ-phase transformed back to the β-phase. Such δ-phase "skeletons" would be expected to exhibit a very high dislocation density.

(3) the brittleness of δ-phase areas where microcracks were commonly observed at the intersections.

Summary

1. β-phase precipitation occurred in the NbH system after electrolytic charging at room temperature in form of large, dendritic particles. Charging at 150°C predominantly led to plates on {100}.
2. β-phase formation belongs to a new metallurgical type of phase transformation here referred to as "hydrogen precipitation".
3. In addition to the usual domain boundaries, β-NbH was found to contain APB's and, under certain conditions, microtwins.
4. δ-phase precipitation (f.c.c. NbH_2) was observed on $\{210\}_{b.c.c.}$ planes inside the β-phase. Between 100 and 200 % coalescence and growth of δ-phase plates occurred until thick δ-phase bands extended through the samples.
5. Hydrogen embrittlement in high concentration NbH alloys is mainly due to the brittleness of the β- and δ-phases and to the formation of microcracks in these phases.

Acknowledgment

The author acknowledges helpful discussions with Drs. H. Wenzl and M.A. Pick. The x-ray powder diffraction work was carried out by Dr. J. Hauck. Dr. J.-M. Welter supported this work through the gas analysis of many samples. Technical assistance was provided by A. Meisenberg, U. Linke, H. Gier, C. Mambor and K.H. Klatt. Thanks are also due to Prof. R. Bourassa for critically reading the manuscript.

References

1. T. Schober, Part II, this issue.
2. T. Schober, Scripta Met. 7, 1119 (1973).
3. R.J. Walter and W.T. Chandler, Trans. MS AIME 233, 762 (1965).
4. M.A. Pick, International Meeting on Hydrogen in Metals, Jül-Conf-6 (1972).
5. M.A. Pick, Ph.D. Thesis, Technische Hochschule Aachen (1973), Jül-Report 951-FF, KFA Jülich.
6. G. Brauer, H. Müller, J. Inorg. Nucl. Chem. 17, 102 (1961). J.J. Reilly, R.H. Wiswall, Jr., Inorg. Chem. 9, 1678 (1970).
7. C. Wainwright, A.J. Cook and B.E. Hopkins, J. Less Common Metals 6, 363 (1964).
8. M.S. Rashid, T.E. Scott, J. Less-Common Metals 30, 399 (1973).
9. T. Schober, M.A. Pick and H. Wenzl, phys. stat. sol. (a) 18, 175 (1973).
10. M. Amano, Y. Sasaki, phys. stat. sol. (a) 19, 405 (1973).
11. D.G. Westlake, W.R. Gray, Appl. Phys. Letters 9, 4 (1966).
12. T. Schober, V. Sorajić, Metallography 6, 183 (1973).
13. H. Wipf, G. Alefeld, phys. stat. sol. (a) 23, 175 (1974).
14. T. Schober, U. Linke, and H. Wenzl, Scripta Met. 8, 805 (1974).
15. V.A. Somenkov, A.V. Gurskaya, M.G. Zemlyanov, M.E. Kost, N.A. Chernoplekov and A.A. Chertkov, Sov. Phys. Sol. State 10, 1076 (1968). V.A. Somenkov, Ber. Bunsenges. physik. Chem. 76, 733 (1972).
16. G. Taylor and J.W. Christian, Phil. Mag. 15, 893 (1967).
17. M.S. Rashid, T.E. Scott, J. Less-Common Metals 31, 377 (1973).
19. G. Alefeld, phys. stat. sol. 32, 67 (1969).
20. B. Alefeld, H.G. Bohn and N. Stump, International Meeting on Hydrogen in Metals, Jül-Conf-6 (Vol. I) p. 286.
21. L.J. von Torne, G. Thomas, Acta Met. 12, 601 (1964).

Figure Captions

Fig. 1: Phase diagram of the NbH system

Fig. 2: Dendritic β-phase particles on the surface of a 100μm single crystal foil after electrolytic charging at room temperature. The SEM image was obtained in the electron microscope with backscattered electrons (40 kV).

Fig. 3: Orthorhombic β-phase
a) Location of hydrogen in tetrahedral positions in real space
b) Reciprocal lattice of β-phase in appropriate orientation to a)

Fig. 4: Straight antiphase boundaries on (100) in β-phase (see arrows). Dark field TEM-image using superlattice reflection of type 1/2 (112).

Fig. 5: Twin lamellae in β-phase as observed after electrolytic charging at 150°C. Habit plane is (211). These twins presumably were produced by plastic deformation during charging procedure.
a) Bright field TEM image. (110) orientation.
b) Dark field TEM image, using strong twin reflection. Approximately same area as in a).
c) SAD pattern and an indexed drawing. Note streaks along $[\bar{2}1\bar{1}]$ in reciprocal space; they arise from thin twin lamellae on $(\bar{2}1\bar{1})$.

Fig. 6: Thin badly deformed β-phase area which is locally warped. Dark bands are the regions with large plastic strain where buckling has occurred.These bands are mainly parallel to traces of {110}, {112} and {123}. Note the large number of microcracks at the intersections of these bands. (The corresponding SAD pattern displayed considerable smearing of the g-vectors by as much as 5 - 10°.)

Fig. 7: Badly deformed β-phase area.
a) Dark high dislocation density bands extend through foil and mark areas where slip has occurred. TEM bright field image, kinematical diffraction conditions.

b) Approximately same area. Dark field image using superlattice reflection 1/2 (21$\bar{1}$) of β-phase. It is seen that the high dislocation density bands in Fig. 7a appear now dark.

Fig. 8: δ-phase (NbH_2) precipitation inside β-phase in form of thin plates on (210) after electrolytic charging. Surfaces were slightly etched with HF and HNO_3 (1:1). Note holes at δ-phase plate intersections as produced by etching. SEM images, using backscattered electrons (80 keV).

a) Initial state of precipitation. Visible are thin δ-plates. (110) single crystal.

b) More advanced state of δ-phase precipitation after coalescence of some of the thinner δ-phase plates; thick δ-plates permeate specimen. (100) single crystal. Estimated concentration: 110 - 120 %.

Fig. 9: Schmematic diagram of β- and δ-phase morphologies in α-matrix, as obtained in UHV-annealed single crystals charged to various concentrations under "equilibrium conditions". Plane of observation: {100}.

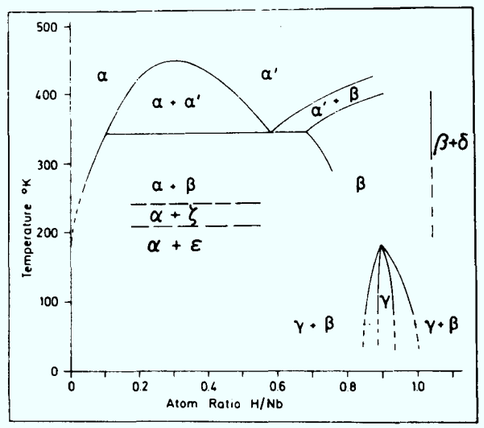
500
400
300
200
100
0
Temperature °K
0
0.2
0.4
0.6
0.8
1.0
Atom Ratio H/Nb
α
α'
α + α'
α' + β
β+δ
α + β
α + ζ
α + ε
β
γ
γ + β
γ + β

Fig. 1

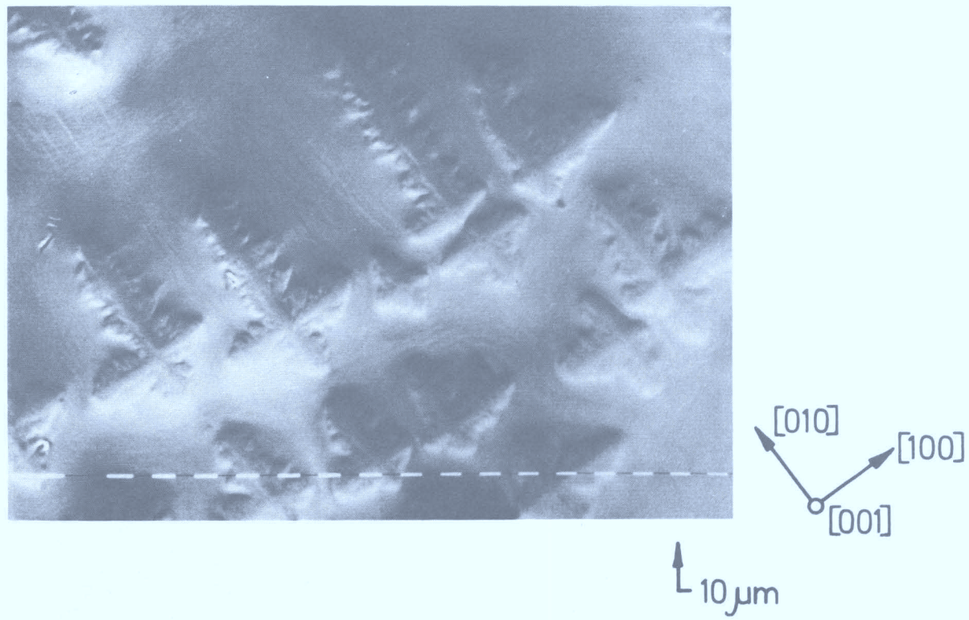

Fig. 2

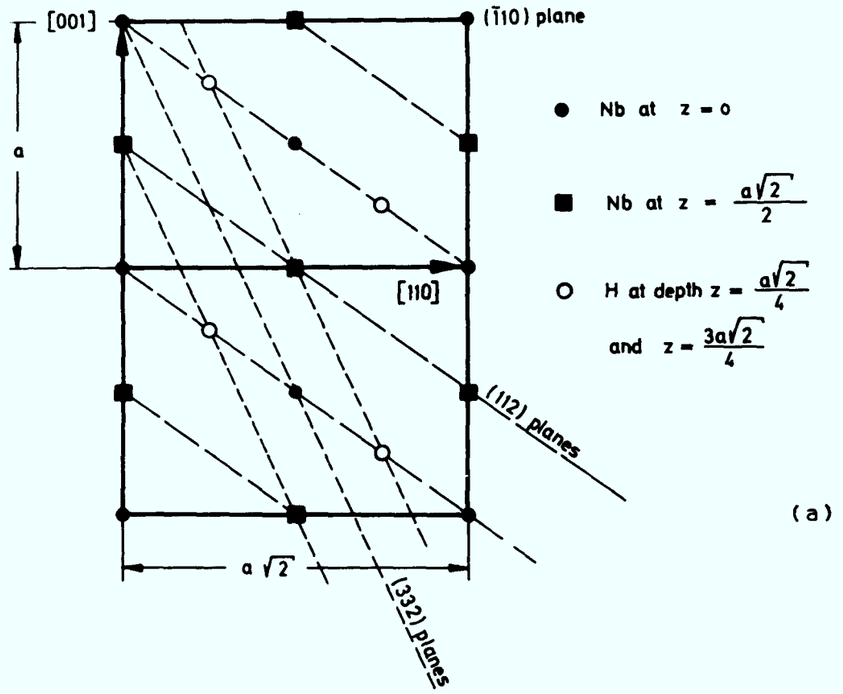
[001]
(1̄10) plane
a
[110]
(112) planes
a √2
(332) planes
Nb at z = 0
Nb at z = a√2/2
H at depth z = a√2/4
and z = 3a√2/4
(a)
002
112
222
000
110
220
1/2(112)
1/2(332)
matrix reflection, z = 0
superlattice reflection, z = 0
matrix reflection
at z = ± √2/2
(b)

Fig. 3

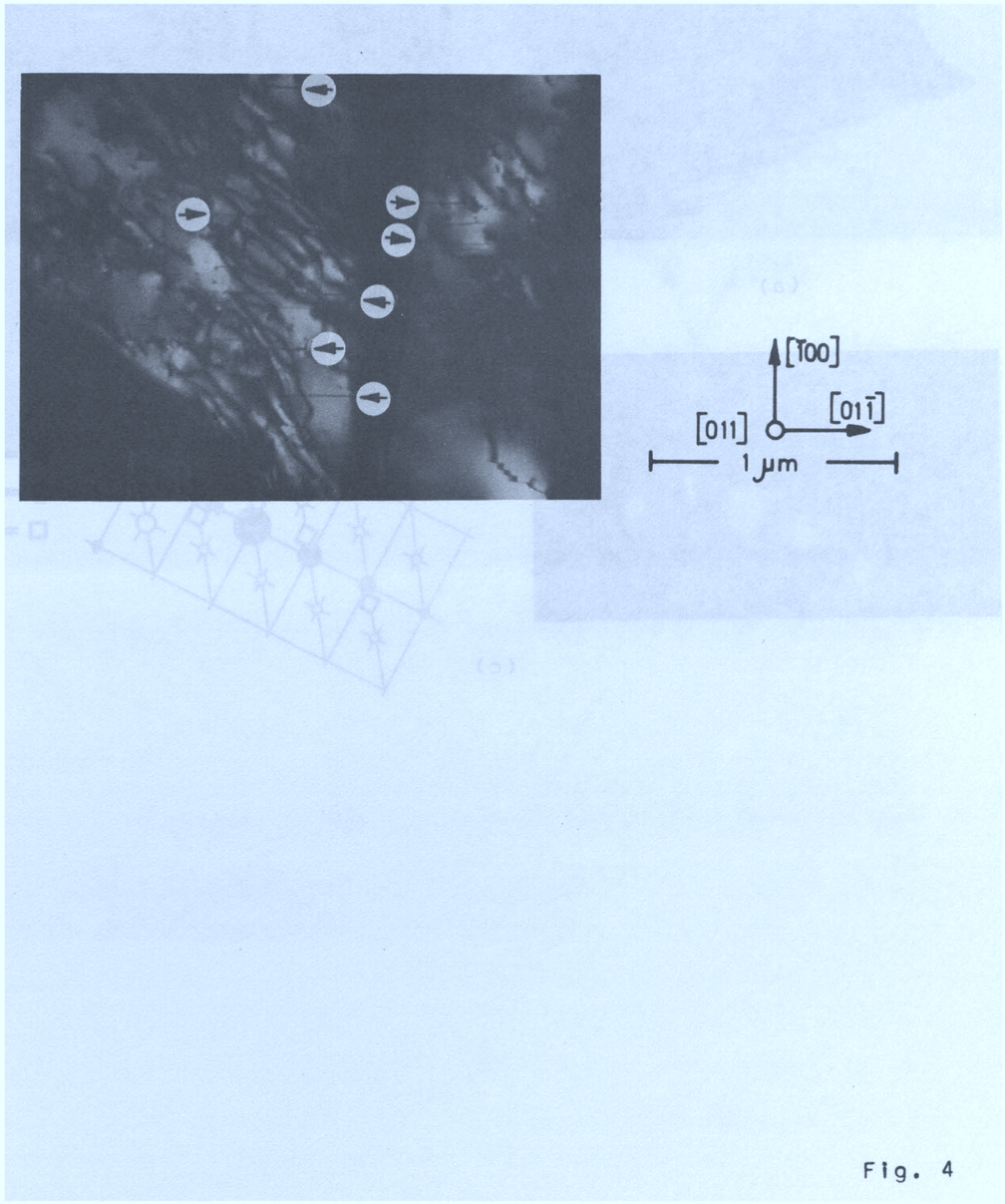

Fig. 4

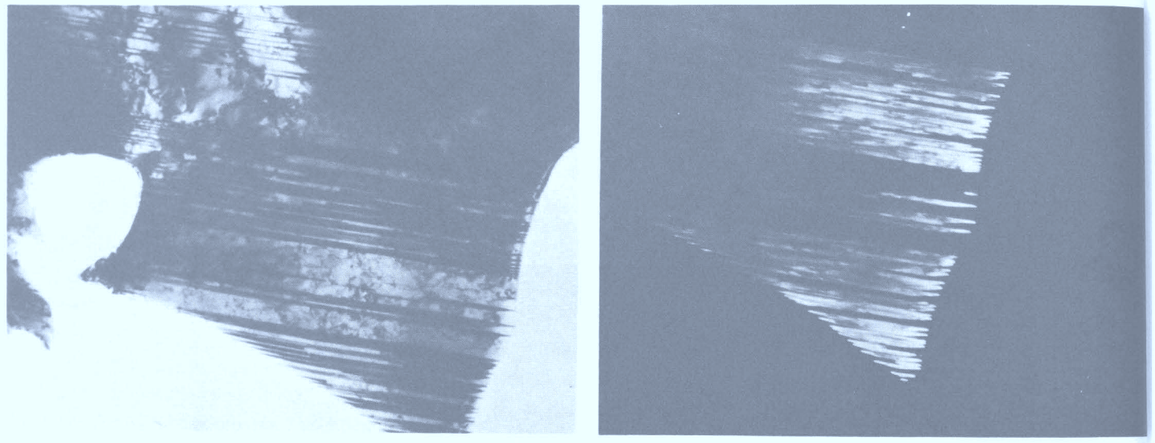

(a) 0,1 µm (b)

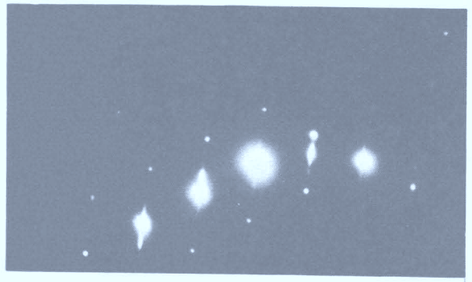

(c)

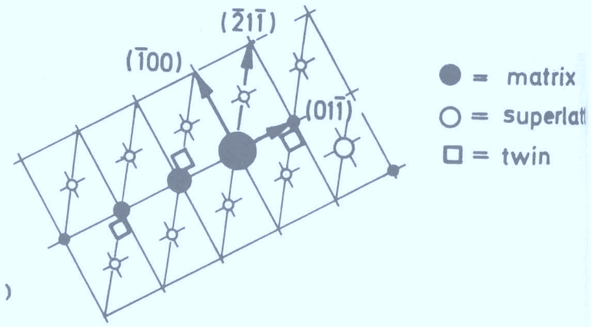

Fig. 5

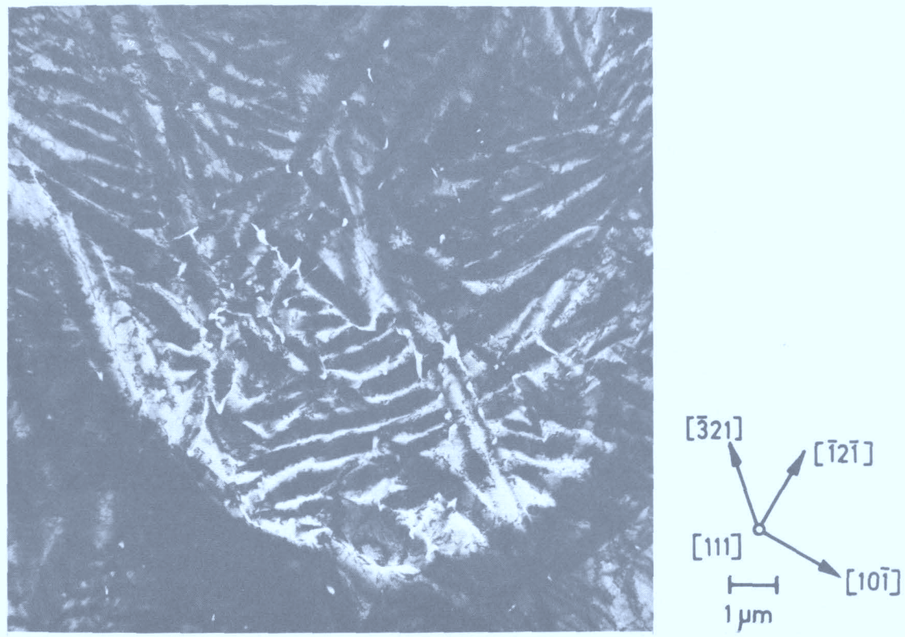

Fig. 6

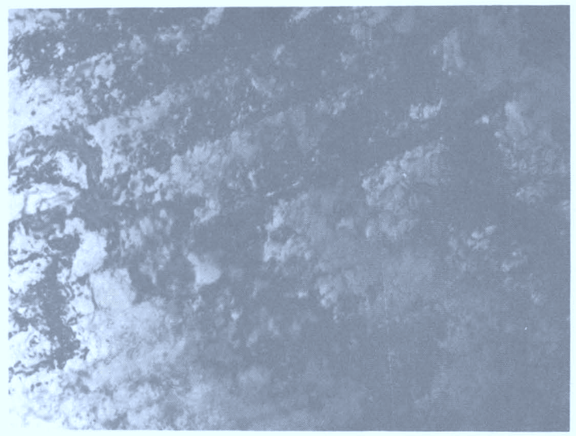

(a)

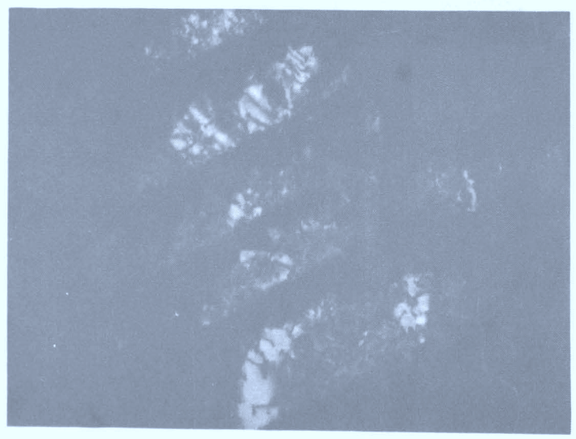

(b)

Fig. 7

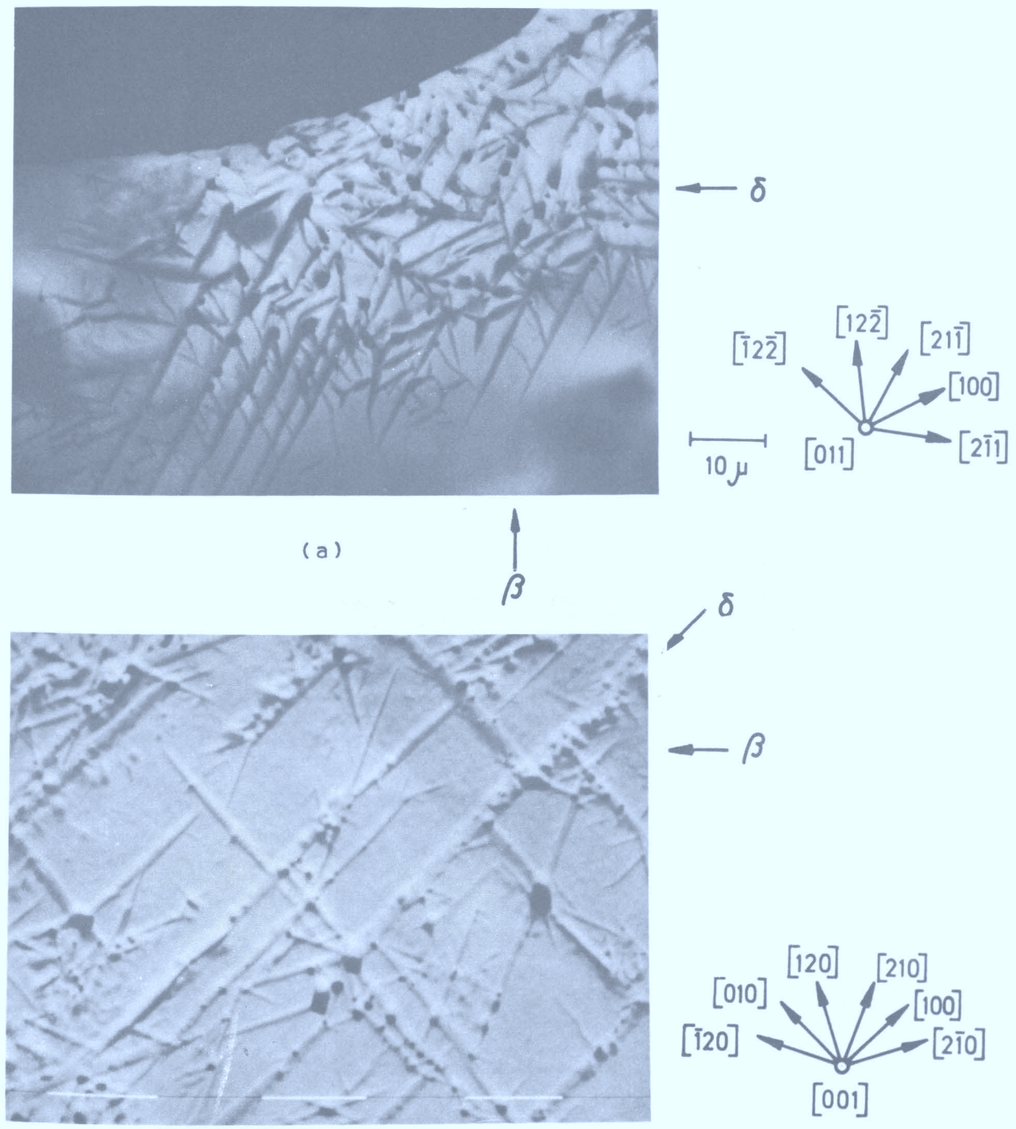
δ
[1̄22̄]
[122̄]
[211̄]
[100]
[2̄11̄]
[011]
10 μ
β
δ
β
[120]
[210]
[010]
[100]
[1̄20]
[2̄10]
[001]
100 μ

(a)

(b)

Fig. 8

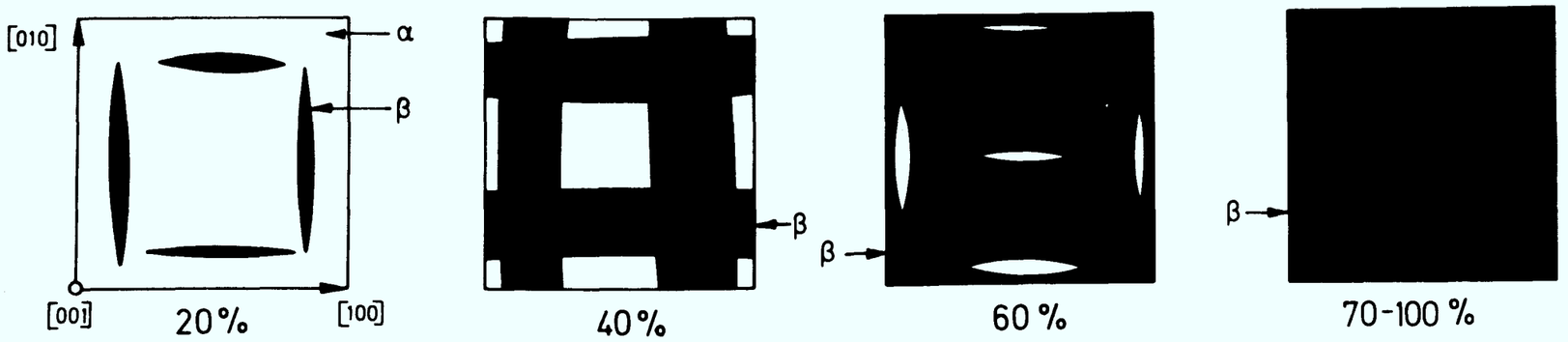
[010]
α
β
[001]
[100]
20 %
β
40 %
β
60 %
β
70-100 %

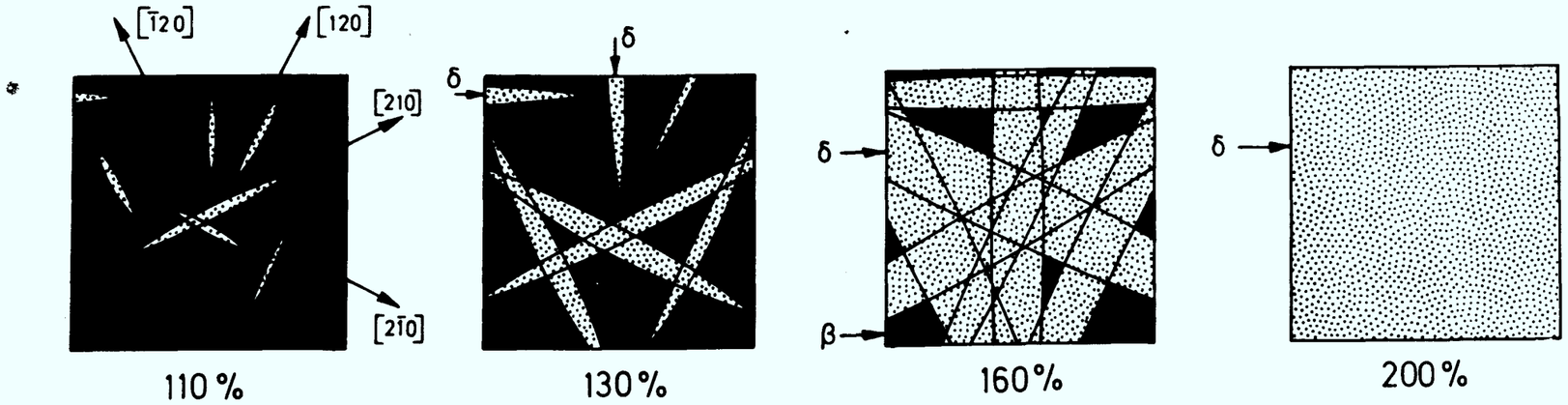
[1̄20]
[120]
[21̄0]
[2̄10]
110 %
δ
δ
130 %
δ
β
160 %
δ
200 %

Fig. 9

Part II

The Niobium Hydrogen System: An Electron Microscope Study
Part II: Low Temperature Structures

T. Schober
Institut für Festkörperforschung
Kernforschungsanlage Jülich, 517 Jülich

Abstract (Part II)

The structure and morphology of low temperature hydride phases was investigated. Quenching of dilute alloys produced small hydride particles which emitted interstitial dislocation loops into the matrix. Irreversible dislocation "skeletons" were generated when such hydride precipitates were thermally dissolved. Three ordered solutions where observed: the β-phase above $-45^{o}C$, the ζ-phase from -45^{o} to $-65^{o}C$ and the ε-phase below $-65^{o}C$. The reciprocal lattices of ζ and ε were determined. The ε-phase is identical with the hydride Nb_4D_3 found by Somenkov /4, 5/. ζ and ε are orthorhombic with the same lattice parameters as β.

1. Introduction

In Part I of this work /1/ an account was given of the room temperature morphology of β- and δ-phase precipitation. It is the purpose of part II to present observations on the morphology and structure of hydrides as formed at low temperatures.
Niobium hydrides have been investigated at low temperatures with x-ray diffraction /2, 3/ and neutron diffraction /4, 5/. Electron diffraction work has mainly centered on the other group Vb metal-hydrides TaH and VH /6-10/.

2. Experimental

The same experimental procedure was followed as outlined in Part I /1/. Electrolytically charged specimens were observed in the cooling holder of a Philips EM 300 G electron microscope. If not stated otherwise, the temperature during observation was approximately -150°C to -160°C.

3. Results

3.1 Precipitation at Low Hydrogen Concentrations

The maximum room temperature solubility of hydrogen in Nb is roughly 5 at % /11/. When the temperature of samples with $c < 5$ % was continuously lowered in the cooling holder of the electron microscope, a sudden appearance of roughly spherical or square shaped hydride precipitates was observed accompanied by bending waves in the sample[1)]. Initially the precipitates were partially coherent and had diameters of tens of nm. Typical examples of the precipitates are shown in fig. 1 where it may be seen that the semicoherent precipitates emitted disloca-

---

1) Once precipitation had occurred at low temperatures, no elastic bending effects could be observed in the α-matrix signifying that most or all of the hydrogen had precipitated.

tion loops and segments along <111>[2]. These dislocation loops which most certainly served to relieve the associated misfit strains, have 1/2 <111> Burgers vectors and are of interstitial character as demonstrated for NbN precipitates /12/. It may be noted that the difference in lattice parameter between the niobium matrix and the resulting orthorhombic hydride is approximately 3.8 % (/2, 3/).

Once dislocation loops had been emitted, a slight rise in temperature caused some of the loops to be re-absorbed by the precipitate. However, loop emission was not fully reversible since the far distant loops and those which had reacted with other dislocations could not be "pulled back" to the emitting precipitate. Precipitation and the conversion of semicoherent to incoherent precipitates occurred in a matter of seconds which may be understood in terms of the very high diffusivity of H in Nb /13/. In fig. 2a, a larger incoherent hydride particle is shown. Initially there was a region in the hydride phase which had twice the diameter of the inner rectangular precipitate as seen in fig. 2a. Warming or the holder led to a shrinkage of the hydride precipitate. We note that the initial shape of the particle may be recognized by the increased dislocation density in the matrix. It was a general observation that whenever a β-phase region transformed into the α-phase a considerable increase occurred in the dislocation density of the area which was "swept" by the α-β phase boundary. Recently it was speculated /14/ that this increase in the dislocation density is due to the formation of sessile $\vec{b}$ = a <100> type dislocations through interactions of b = $\frac{a}{2}$ <111> type dislocations which form the migrating phase boundary. Thus any dissolved hydride particle was observed to leave behind a dislocation "skeleton"

---

2) Precipitation increases the local atomic density. Therefore, material must be transported away from the precipitation sites. This is accomplished by the emission of interstitial dislocation loops which can glide away along a cylinder defined by their Burgers vector. Aside from punched-out loops, precipitation in dilute alloys resulted in a considerable amount of plastic deformation in the matrix as is shown by families of long screw dislocations on different slip planes (see for this point fig. 1a of /1/).

outlining the shape of the previous hydride precipitate (see also Ref. /14, 15/). The "skeletons" themselves are further subdivided into cells separated by dislocation walls and tangles. These cells have slightly different orientations and are the main cause for the mosaic spread observable by TEM or x-ray techniques /16/ in such specimens. A typical example of such a dislocation skeleton and its essential features is presented in fig. 2b.
Initially a square shaped hydride particle - as marked by A-B-C-D - was produced by quenching a 5 % NbH alloy into liquid nitrogen. Upon warming to room temperature, the hydride particle dissolved, producing the skeleton seen in fig. 2b. Dissolution has started somewhere at the four sides. The dislocation tangles along AE, BE, CE, DE mark where the fronts of the advancing phase boundaries have met. SAD experiments showed that the cells AEB, BEC, CED and AED all have slightly different orientations among themselves and also with respect to the matrix.

Cycling the temperature repeatedly above and below the phase boundary established that the hydrides precipitate often (but not exclusively) at the dislocation "skeletons" left behind in the previous cycles. It was found that continued cycling gradually increased the content of "skeletons" in the matrix and thereby the dislocation density in the specimen. (At higher concentrations, similar cycling was observed to lead to microcracks in the high dislocation density areas.)

Furthermore, domain boundaries were also observed in the smaller hydride particles. They arise from the orthorhombic hydride structures as discussed in detail in /17, 18/. A diffraction analysis of the hydrides is presented below; it may be noted here that selected area diffraction patterns (= SAD's) of small hydrides showed the appearance of new, slightly shortened $\vec{g}$-vectors due to the precipitates. This effect may be seen in fig. 3. The observed values of $\Delta g/g$ were all negative and in accordance with the above difference in lattice parameter of 3.8 %. Moiré fringes could also be observed under suitable

diffraction conditions and had spacings which were in agreement with the above value.

3.2 Precipitation at Elevated Hydrogen Concentrations and Diffraction Analysis

At higher concentrations, large irregularly shaped patches could be observed (see Part I /1/) which were completely in the hydride phase and were well suited for a SAD analysis of areas comprising only one domain of the hydride phase. It was soon observed that a new set of superlattice reflections appeared below $-65^{o}C$, indicating that a phase transformation had taken place at this temperature. This new phase has been referred to as the ε-phase /1/. According to Somenkov /4, 5/ the stoichiometric phase Nb_4D_3 can be observed below $-103^{o}C$. It has a composition of 75 %, belongs to the space group $P2_12_12_1$ in the orthorhombic system and is non-centrosymmetric. The Nb_4D_3 structure is shown in fig. 4. The unit cell has the size $a \approx b \approx 2a_o\sqrt{2}$ and $c \approx a_o$ (a_o lattice parameter of pure Nb). It is obtained from the β-phase by a periodic arrangement of the vacancies in the interstitial "hydrogen crystal". The Nb_4D_3 reciprocal lattice is seen in fig. 5.

In order to compare the reciprocal lattices of the ε-phase (as determined by electron diffraction) and the Nb_4D_3 structure, a series of tilting experiments was performed on one domain of the ε-phase: Tilts were carried out about a 001 [3] axis resulting in (100)-(310)-(210) and (110) reciprocal lattice sections as shown in fig. 6. A continuous scan of reciprocal space was thus possible as described in /18/. The resulting complete reciprocal lattice of the ε-phase as determined from SAD's was found to be the same as Somenkov's reciprocal lattice of the Nb_4D_3 structure in fig. 5 /4/. It was therefore concluded that the ε-phase is identical with the Nb_4D_3 compound found by Somenkov /4, 5/. Additional reciprocal lattice sections (other than the planes cited above) were all in agreement with the model in fig. 5.

---

[3] As in Part I /1/, all indices are given in b.c.c. notation.

Several observations support the conclusion that the ε-phase has the same orthorhombic crystal structure and (within the limits of experimental error) the same lattice parameters as the β-phase:

1. Boundaries between β and ε regions have the character of twin or domain boundaries and are imaged as δ-fringes /17/. No signs for coherency strains or even dislocation boundaries were detected. The nucleation and growth of ε-phase particles within the β-phase was also strain free as shown in fig. 7 (for details, see figure caption).
2. No evidence for the splitting up of high order $\vec{g}$-vectors was found in the SAD's taken from areas containing both the β- and ε-phase.
3. Triple junctions of domain boundaries were observed in the ε-phase (as well as in the β-phase) proving the existence of three preferred orientations in the ε-phase.

The above conclusions were also supported by x-ray evidence in the work of Pick /2, 3/ where no change in the positions of the orthorhombic reflections of the metal lattice was observed when cooling down NbH specimens below -65°C. The domain boundaries in the ε-phase were similar to the boundaries observed in the β-phase. Typical examples are shown in fig. 8a, b (for details see figure caption). Dark field observations in the ε-phase using superlattice reflections were exceedingly difficult because of the low intensity of the various beams. The β→ε transformation was found to occur rather slowly since large patches of the β-phase could still be observed at a temperature of -150°C.

3.3 Observations within the ζ-phase

When areas containing the ε-phase are warmed up in the electron microscope above -65°C, a sudden disappearance of some of the superlattice reflections of the ε-phase was observed. The remaining set of reflections was of the type 1/2 (110). This disappearance was ascribed to still a new phase transition, re-

sulting in the ζ-phase /1/. A (001) section (SAD) of the ζ-phase reciprocal lattice section is shown in fig. 9a, whereas in fig. 9b a tentative reciprocal lattice is presented as determined from several SAD's. Clearly, the ζ-phase reciprocal lattice is obtained from the one of the ε-phase by omitting a number of superlattice reflections. This signifies that above -65°C the complete order of the Nb_4H_3 structure is destroyed resulting in a state of lesser order, the ζ-phase, which in turn is still in a higher degree of order than the β-phase.

At -45°C, the ζ reflections disappeared resulting in the usual β-phase SAD's. No apparent change was observed in the specimen in bright field when going through the ε→ζ and ζ→β transitions. The domain structure of the ζ-phase was found to be identical to the one prevailing in the ε-phase.

4. Discussion

Precipitation at low concentrations and low temperatures was found to lead to plastic deformation of the specimen. This may explain the degradation of highly perfect Nb single crystals containing hydrogen in solution when cooled below the phase boundary. Since dislocation walls forming the α-β phase boundary of β-phase precipitates do not glide out of the specimen when it is heated above the solubility limit, but essentially stay behind in a disordered state and form the "dislocation skeleton", the original perfection of hydrogen-containing Nb crystals cannot be restored by warming up to higher temperatures. The above effect may therefore be referred to as "precipitation damage" by the precipitating hydrogen.

The present observations are in support of the results by Westlake /15/ who found low temperature ductility for rapidly cooled NbH specimens. This effect was explained by the production of prismatic dislocation loops and the generation of very small hydride particles. Both points could be proved in the present work where essentially fast cooling rates were used.

The present results demonstrate that there are three distinct ordering states for NbH alloys, the phases β,ζ and ε. At -45°C, the β-phase transformed into the ζ-phase, accompanied by an enlargement of the unit cell and partial ordering of the vacancies in the "interstitial hydrogen crystal". The real crystal structure of the ζ-phase could not be determined in the present work since electron diffraction does not provide any intensity information on the superlattice reflections which is required for an unambiguous structural analysis. Further ordering occurred below -65°C where the ε-phase (the compound Nb_4H_3) was observed. Its composition of 75 % expresses the tendency towards stoichiometry at low temperatures /4/. The reasons why Somenkov et al. /4/ observed the appearance of the ε-phase only at -103°C (seen at -65°C in this work) are not clear as yet[4].

The β→ζ and ζ→ε transitions at -45°C and -65°C were unknowingly observed by several authors. Amano et al. /19/ found distinct peaks at -70° and -35°C in internal friction, electrical resistivity and DTA measurements of a 43 % NbH alloy. Buck et al. /11/ reported a sharp internal friction peakt at -43°C. Ableiter /20/ concluded on the basis of resistivity and Mössbauer measurements that a phase transition occurred in β-NbH between -96°C and -76°C.

5. Summary

1. At low concentration hydrogen precipitated upon rather rapid cooling in form of small, roughly spherical or square shaped particles, leading to local plastic deformation and the emission of interstitial prismatic dislocation loops (generation of "precipitation damage").

---

4) Presumably, experimental difficulties in the neutron diffraction work have led to this discrepancy. It is unlikely that there is such a distinct isotope effect to account for this large temperature difference.

2. When the hydrogen precipitates were dissolved again, dislocation "skeletons" remained at the site of the previous hydride particles. These skeletons consisted of regions of slightly different orientations.
3. Three ordered NbH phases were observed in the following temperature ranges: β above -45°C, ζ from -45° to -65°C, ε below -65°C (presumably metastable β-NbH was also observed below -65°C).
4. The reciprocal lattices of the ζ- and ε-phases were determined. The ε-phase is identical with the compound Nb_4D_3 found by Somenkov /4/. Evidence for an orthorhombic structure of ζ- and ε-phase with the same lattice parameter as the β-phase was presented.

References

1. T. Schober, Part I this issue;
   T. Schober, Scripta Met. 7, 1119 (1973).
2. M.A. Pick, Ph.D. Thesis, Technische Hochschule Aachen (1973);
   Jül-Report 951-FF, KFA Jülich.
3. M.A. Pick, International Meeting on Hydrogen in Metals;
   Jül-Conf-6 (1972).
4. V.A. Somenkov, A.V. Gurskaya, M.G. Zemlyanov, M.E. Kost,
   N.A. Chernoplekov and A.A. Chertkov, Sov. Phys. Sol. State
   10, 1076 (1968).
5. V.A. Somenkov, Ber. Bunsenges. physik. Chem. 76, 733 (1972).
6. J. Wanagel, S.L. Sass, and B. Batterman, phys. stat. sol. (a)
   10, 49 (1972); 11, K 97 (1972);
   Metall. Trans. 5, 105 (1974).
7. S. Takano, T. Suzuki, Acta Met. 22, 265 (1974).
8. T. Chiba, S. Takano, J. Phys. Soc. Japan 31, 1113 (1971).
9. M. Cambini, R. Serneels and R. Gevers, phys. stat. sol. (a)
   21, K 57 (1974).
10. H. Asano, M. Hirabayashi, phys. stat. sol. (a) 16, 69 (1973);
    15, 267 (1973).
11. O. Buck, D.O. Thompson and C.A. Wert, J. Phys. Chem. Solids
    32, 2331 (1971).
12. N. Dahlstrom, B.L. Eyre, Metal Sci. J. 6, 96 (1972).
13. J. Völkl, G. Schaumann and G. Alefeld, J. Phys. Chem. Solids
    31, 1805 (1970).
14. M. Amano, Y. Sasaki, phys. stat. sol. (a) 19, 405 (1973).
15. D.G. Westlake, Trans. TMS-AIME 245, 1969 (1969).
17. H. Wenzl, private communication.
17. S. Amelinckx, Surface Science 31, 296 (1972).
18. T. Schober, M.A. Pick and H. Wenzl, phys. stat. sol. (a)
    18, 175 (1973).
19. M. Amano, T. Matsumoto and Y. Sasaki, Scripta Met. 7, 371
    (1973).
20. M. Ableiter, Ph.D. Thesis, University of Saarbrücken (1973).

Figure Captions (Part II)

Fig. 1: Semicoherent hydride precipitates in a dilute NbH alloy cooled down to -160°C inside the electron microscope. The particles are seen to emit prismatic dislocation loops along <111>. Kinematical TEM image.

Fig.2a: Rectangular hydride particle in a dilute NbH alloy. The corners are marked by arrows. Note domain boundary in right side of the particle. The precipitate has shrunk from its original, double size, leaving behind a high concentration of dislocations. TEM image.

Fig.2b: STEM-image of dislocation skeleton as produced by quenching a dilute NbH alloy into liquid nitrogen and subsequent warming. A, B, C and D mark corners of original hydride precipitate. Triangles AEB, BEC, CED and AED are separated by dislocation tangles and have slightly different orientations. Note the drastic increase in dislocation density in the skeleton (Voltage: 80 keV, foil thickness $\approx$ 2000 Å, observation at room temperature.

Fig. 3: (110) SAD pattern of dilute NbH alloy containing hydride precipitates. Photographed at -160°C. Matrix reflections are surrounded by new shortened and smeared-out reflections which are due to hydrides. Smearing is caused by the domain structure and plastic deformation of the precipitates and the surrounding matrix.

Fig. 4: Model of Nb_4D_3 structure (after Somenkov et al. /4, 5/). The hydrogen atoms occupy tetrahedral positions. A long period superlattice arises from the ordering of vacancies.

Fig. 5: Reciprocal lattice of the Nb_4D_3 structure (after Somenkov et al. /4, 5/).

Fig. 6: SAD's resulting from a tilting experiment in reciprocal space performed on one domain of the ε-phase. Tilts around [001] produce (100)-(310)-(210) and (110) sections of the reciprocal lattice in Fig. 5.

Fig. 7: Strainfree ε-phase precipitates inside β-phase. Precipitates have shape of rectangular prisms bounded by (100) and (110) planes.

a) TEM bright field image. Arrows depict ε-precipitates with bright contrast.

b) TEM dark field image of the same area using a superlattice reflection of the β-phase. ε-particles appear now dark.

Fig. 8: Domain boundaries in the ε-phase running in a zig-zag fashion through the specimen. They separate regions which are slightly tilted. Domain boundaries have "δ"-type fringe contrast /17/.

a) TEM bright field image. Two beam conditions $s \approx 0$.

b) TEM dark field image of same area. Two beam conditions, $s \approx 0$. Note alternating contrast of domain boundaries: either black or white stripes are observed. This signifies that boundaries produce tilts in mutually opposite directions. The net tilt over a larger distance remains zero.

Fig. 9: Reciprocal lattice of ζ-NbH phase

a) (002)-SAD pattern of ζ-phase

b) Reciprocal lattice as determined from several SAD's. Compare (002) plane with a).

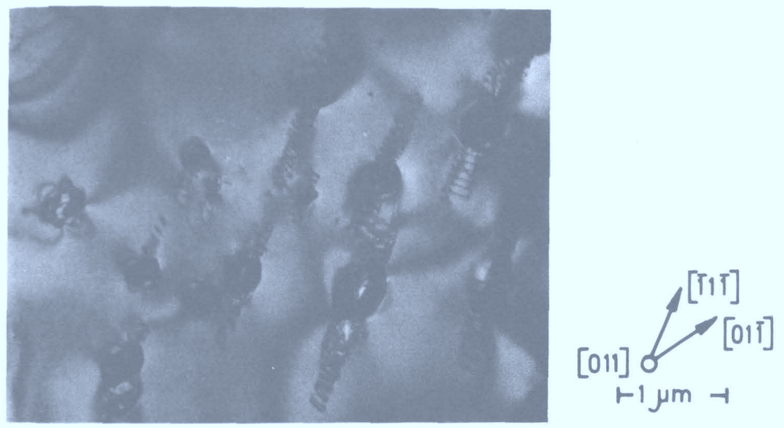

Fig. 1

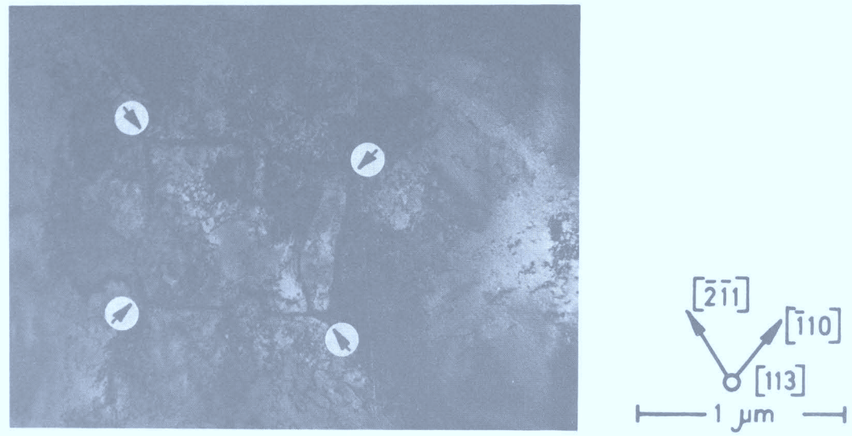

Fig.2a

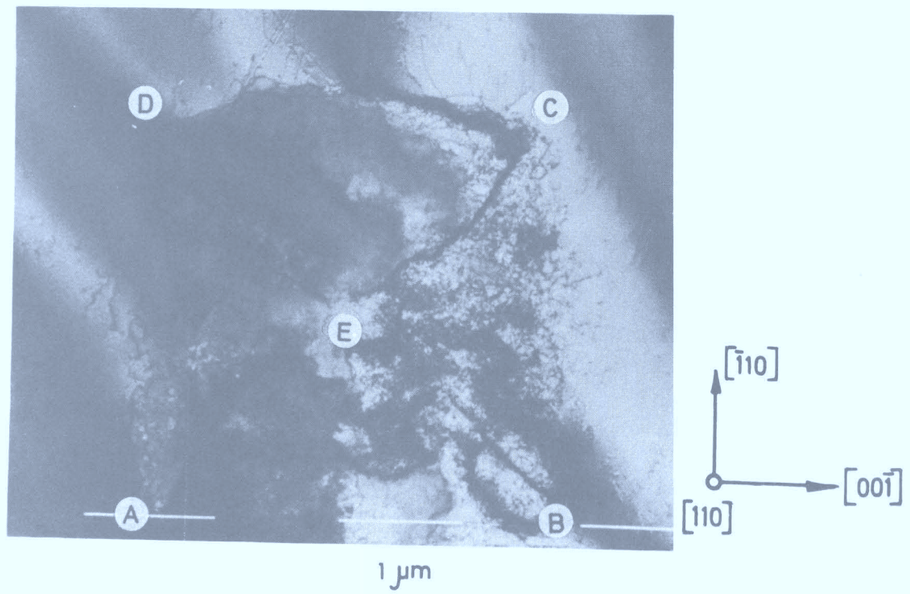

Fig.2b

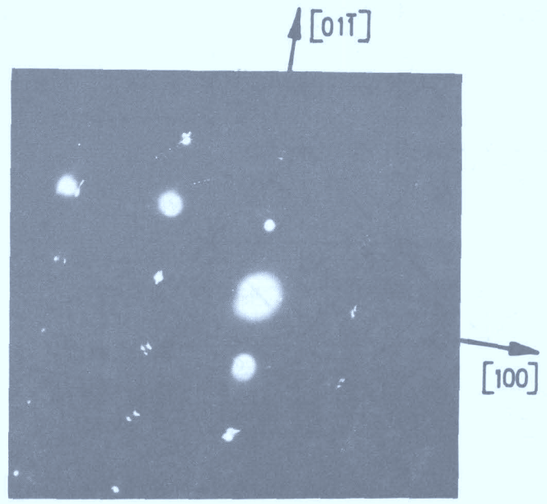

Fig. 3

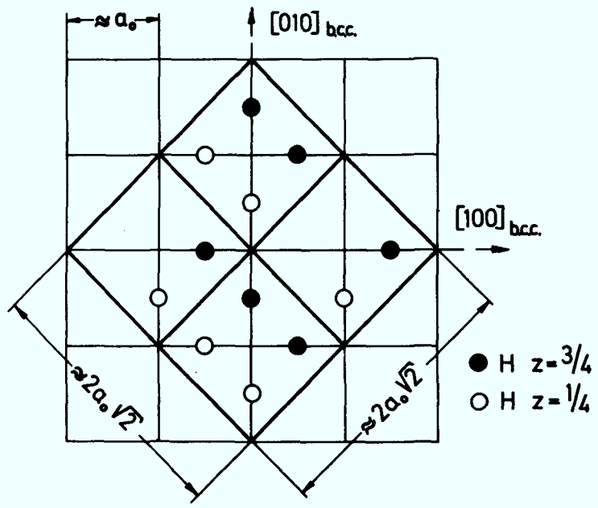

Fig. 4

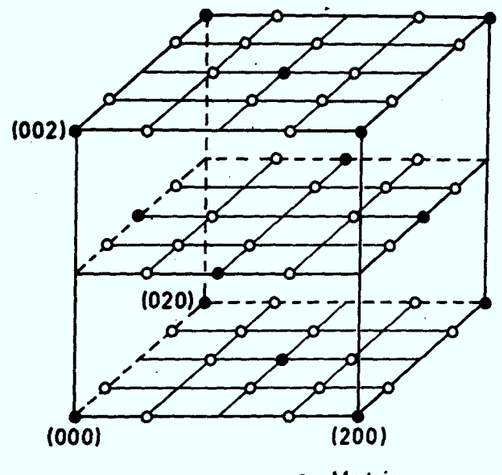

Fig. 5

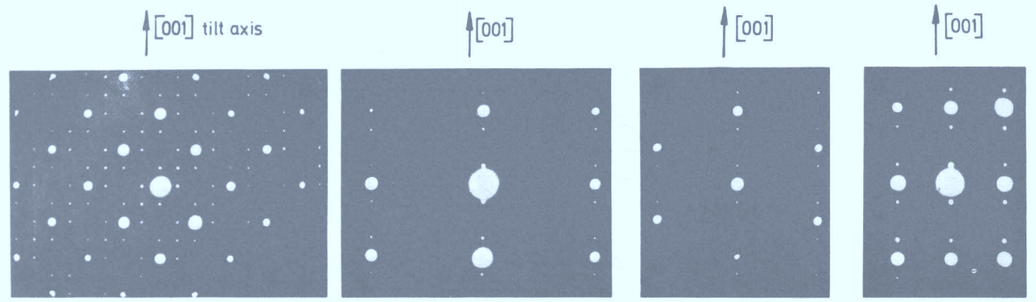

Fig. 6

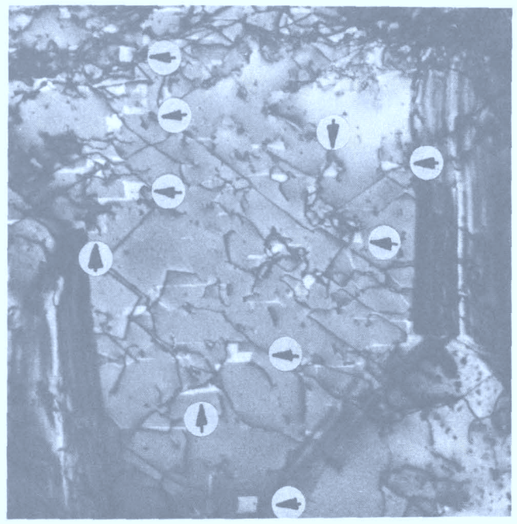

(a)

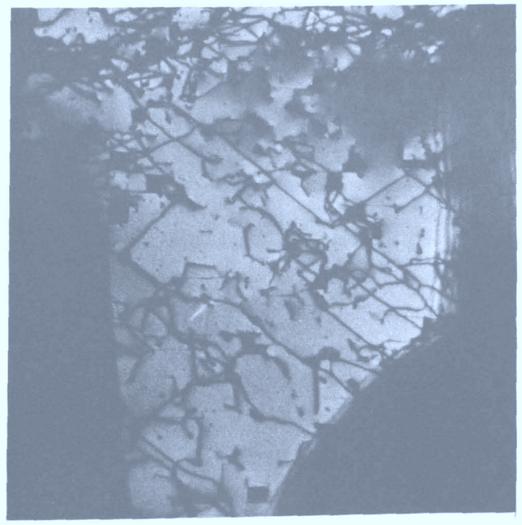

(b)

Fig. 7

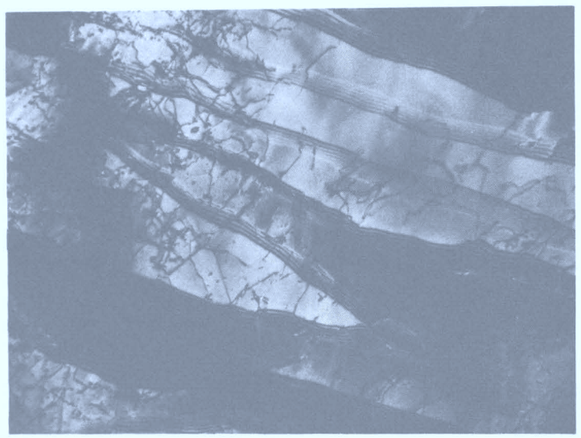

(a)

(b)

Fig. 8

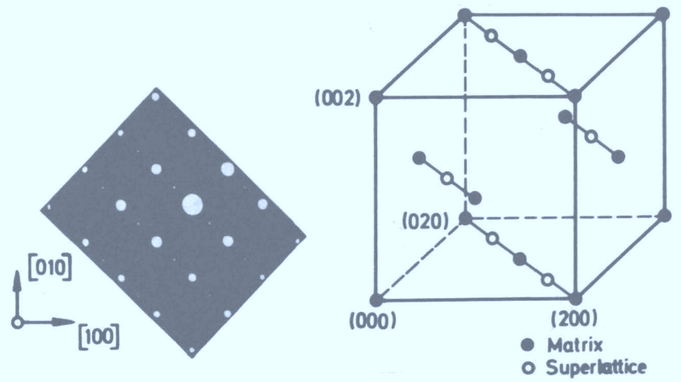

Fig. 9